Commun. Math. Res.
doi: 10.4208/cmr.2020-0013

Vol. **36**, No. 3, pp. 247-271
August 2020

Moving-Water Equilibria Preserving HLL-Type Schemes for the Shallow Water Equations

Christian Klingenberg[1], Alexander Kurganov[2], Yongle Liu[2,3,*] and Markus Zenk[1]

[1] *Institute for Mathematics, Würzburg University, Würzburg 97074, Germany.*
[2] *Department of Mathematics and SUSTech International Center for Mathematics, Southern University of Science and Technology, Shenzhen 518055, China.*
[3] *Department of Mathematics, Harbin Institute of Technology, Harbin 150001, China.*

Received 3 April 2020; Accepted 22 June 2020

Abstract. We construct new HLL-type moving-water equilibria preserving upwind schemes for the one-dimensional Saint-Venant system of shallow water equations with nonflat bottom topography. The designed first- and second-order schemes are tested on a number of numerical examples, in which we verify the well-balanced property as well as the ability of the proposed schemes to accurately capture small perturbations of moving-water steady states.

AMS subject classifications: 76M12, 65M08, 35L65, 86-08, 86A05

Key words: Shallow water equations, Harten-Lax-Van Leer (HLL) scheme, well-balanced method, steady-state solutions (equilibria), moving-water and still-water equilibria.

*Corresponding author. *Email addresses:* liuyl2017@mail.sustech.edu.cn (Y. Liu), klingen@mathematik.uni-wuerzburg.de (C. Klingenberg), alexander@sustech.edu.cn (A. Kurganov), markus.zenk@mathematik.uni-wuerzburg.de (M. Zenk)

1 Introduction

In this paper, we develop a new numerical method for the Saint-Venant system of shallow water equations. The Saint-Venant system is a hyperbolic system of balance laws, which was developed in [11] and still used in a wide variety of applications related to modeling water flows in rivers, canals, lakes, coastal areas and even in deep oceans in the situations in which the horizontal length scale is much greater than the vertical length scale. In the one-dimensional (1-D) case, the Saint-Venant system reads as

$$\begin{cases} h_t+(hu)_x=0, \\ (hu)_t+\left(hu^2+\frac{g}{2}h^2\right)_x=-ghB_x, \\ B_t=0, \end{cases} \tag{1.1}$$

where x and t are the spatial and temporal variable, respectively, $h=h(x,t)$ is the water depth, $u=u(x,t)$ is the velocity, $B=B(x)$ is the bottom topography assumed to be time-independent, and g is acceleration due to gravity.

The Jacobian of the system (1.1) has three eigenvalues $\lambda_\pm(h,u)=u\pm\sqrt{gh}$ and $\lambda_0=0$. Therefore, the system (1.1) is hyperbolic as long as $h\geq 0$ and is strictly hyperbolic if $\lambda_+\lambda_-\neq 0$. There are three possible flow regimes depending on the above eigenvalues: (i) if $\lambda_-\lambda_+<0$ then the flow is *subcritical*, (ii) if $\lambda_+\lambda_->0$ then the flow is *supercritical*, (iii) if $\lambda_+\lambda_-=0$ then the flow is *critical*. It is easy to show that the system (1.1) admits the following equilibria:

$$q:=hu\equiv\text{Const},\quad E:=\frac{u^2}{2}+g(h+B)\equiv\text{Const}, \tag{1.2}$$

where q and E denote the discharge and total energy, respectively. The steady states (1.2) are of great practical importance as many physically relevant water waves are, in fact, their small perturbations. "Lake at rest" steady states or still-water equilibria given by

$$u\equiv 0,\quad h+B\equiv\text{Const}, \tag{1.3}$$

form a subclass of (1.2). When $u\not\equiv 0$, the steady states (1.2) are called moving-water equilibria.

It is well-known that a good numerical method for the Saint-Venant system (1.1) should be capable of exactly preserving all of the equilibria given by (1.2) or at least the still-water equilibria (1.3). Such schemes are called *well-balanced* as they respect a delicate balance between the flux and source terms in the discharge

equation in (1.1). Derivation of well-balanced schemes for the shallow water equations has been an active area of research since the pioneering works [2] and [16]. Numerous still-water equilibria preserving schemes have been developed [1, 4, 5, 7, 13, 18–21, 26, 28]. Further research has been done to construct moving-water equilibria preserving schemes [3, 6, 8–10, 19, 24, 27, 31–34]. An advantage of moving-water equilibria preserving schemes over their still-water equilibria preserving ones has been clearly demonstrated in [9, 10, 19, 33].

In this paper, we rigorously derive a simple moving-water equilibrium preserving extension of the Harten-Lax-van Leer (HLL) scheme, originally developed for hyperbolic systems of conservation laws in [17], to the 1-D Saint-Venant system (1.1). We proceed along the lines of the HLL-type scheme recently introduced in [12] for the compressible Euler equations with gravity. The HLL-type scheme presented here is close to the numerical schemes derived in [3, 24], which were constructed under the assumption that the flow is subcritical. We, however, focus on extending the HLL-type approach to all possible flow regimes. The novelty of our scheme is also in solving the cubic equation that needs to be solved to compute the values of h given the values of the equilibrium variables q and E. While in the aforementioned papers, this was done approximately using Newton's method (which may or may not converge, especially near the critical points in transcritical flow regimes), we work out the required details and use the exact solution.

The paper is organized as follows. In Section 2, we present the HLL-type approximate Riemann problem solver for different flow regimes. In Section 3, we introduce the first-order numerical scheme based on the previously developed approximate Riemann problem solver. We also investigate the well-balanced properties of the designed scheme and introduce its second-order extension. In Section 4, we describe the exact solver for the cubic equation that relates the equilibrium and conservative variables. Finally, in Section 5, we report the results of several numerical experiments designed to demonstrate the performance of the proposed HLL-type schemes.

2 HLL-type approximate Riemann problem solver

In this section, we derive the HLL-type approximate solution of the Riemann problem for the Saint-Venant system (1.1) subject to the following initial data:

$$\boldsymbol{w}(x,0)=\begin{cases}\boldsymbol{w}_L, & x<0,\\ \boldsymbol{w}_R, & x>0,\end{cases}\qquad \boldsymbol{w}=(h,q,B)^\top \tag{2.1}$$

with the prescribed values of $\boldsymbol{w}_L := (h_L, q_L := h_L u_L, B_L)^\top$ and $\boldsymbol{w}_R := (h_R, q_R := h_R u_R, B_R)^\top$. We also introduce the corresponding energy values

$$E_L := \frac{u_L^2}{2} + g(h_L + B_L), \quad E_R := \frac{u_R^2}{2} + g(h_R + B_R).$$

Since we need a Riemann problem solver for all three flow regimes, we will study each of them separately.

Before designing the HLL-type Riemann problem solver, we introduce the signal speeds

$$\lambda_L = \min\{\lambda_-(h_L,u_L), \lambda_-(h_R,u_R)\}, \quad \lambda_R = \max\{\lambda_+(h_L,u_L), \lambda_+(h_R,u_R)\}.$$

Depending on the signs of λ_L and λ_R, we will distinguish between the supercritical, subcritical and critical cases.

2.1 Supercritical case

We begin with the supercritical case. For symmetry reasons, it is enough to analyze the case of two positive eigenvalues ($\lambda_L > 0$ and $\lambda_R > 0$). We therefore seek an approximate solution in the following form:

$$\boldsymbol{\mathcal{W}}_{\sup}(x,t) = \begin{cases} \boldsymbol{w}_L, & \text{if} \quad \frac{x}{t} < 0, \\ \boldsymbol{w}_L^*, & \text{if} \quad 0 < \frac{x}{t} < \lambda_L, \\ \boldsymbol{w}_R^*, & \text{if} \quad \lambda_L < \frac{x}{t} < \lambda_R, \\ \boldsymbol{w}_R, & \text{if} \quad \lambda_R < \frac{x}{t}. \end{cases} \tag{2.2}$$

We note that the evolution of the bottom topography satisfying the trivial equation $B_t = 0$ is decoupled from the evolution of h and q. Therefore, $B_L^* = B_R^* = B_R$, and one has to determine the remaining four unknowns h_L^*, h_R^*, q_L^* and q_R^*; see Fig. 1, where the function $\boldsymbol{\mathcal{W}}_{\sup}(x,t)$ is schematically presented in the (x,t)-plane on the rectangle $[-\frac{\Delta x}{2}, \frac{\Delta x}{2}] \times [0, \Delta t]$ with $\Delta x > 0$ being a fixed (small) number and $\Delta t > 0$ determined using the CFL condition with the CFL number $\frac{1}{2}$, namely, $\lambda_R \mu \le \frac{1}{2}$, where $\mu := \frac{\Delta t}{\Delta x}$.

We first use the consistency relation

$$\frac{1}{\Delta x} \int_{-\Delta x/2}^{\Delta x/2} \boldsymbol{\mathcal{W}}\left(\frac{x}{\Delta t}, \boldsymbol{w}_L, \boldsymbol{w}_R\right) \mathrm{d}x = \frac{1}{\Delta x} \int_{-\Delta x/2}^{\Delta x/2} \boldsymbol{W}\left(\frac{x}{\Delta t}, \boldsymbol{w}_L, \boldsymbol{w}_R\right) \mathrm{d}x, \tag{2.3}$$

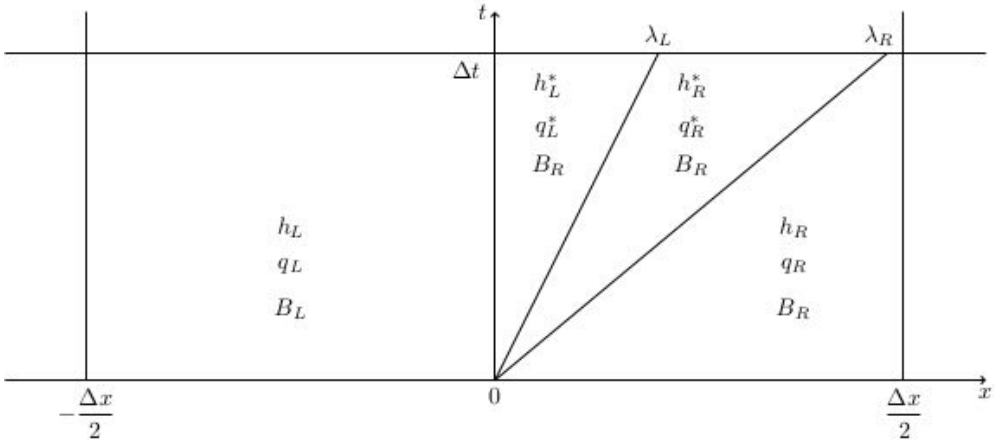

Figure 1: Structure of the HLL-type approximate Riemann problem solver $\mathcal{W}_{\text{sup}}(x,t)$.

where W is the exact solution of the Riemann problem (1.1), (2.1) and $\mathcal{W}=\mathcal{W}_{\text{sup}}$. This gives

$$\begin{aligned}&\frac{1}{2}h_L+\lambda_L\mu h_L^*+(\lambda_R-\lambda_L)\mu h_R^*+\left(\frac{1}{2}-\lambda_R\mu\right)h_R\\ =&\frac{1}{2}(h_L+h_R)-\mu(q_R-q_L),\end{aligned}\tag{2.4}$$

$$\begin{aligned}&\frac{1}{2}q_L+\lambda_L\mu q_L^*+(\lambda_R-\lambda_L)\mu q_R^*+\left(\frac{1}{2}-\lambda_R\mu\right)q_R\\ =&\frac{1}{2}(q_L+q_R)-\mu\left(h_Ru_R^2+\frac{g}{2}h_R^2-h_Lu_L^2-\frac{g}{2}h_L^2\right)-\mu\overline{ghB_x},\end{aligned}\tag{2.5}$$

where $\overline{ghB_x}$ is a discretization of the source term, which will be determined in Section 3.1.1 from the well-balanced requirement. In order to obtain two additional equations, we impose the equilibrium relations across the stationary λ_0-wave, that is, we require

$$q_L^*=q_L,\quad \frac{1}{2}\left(\frac{q_L^*}{h_L^*}\right)^2+g(h_L^*+B_R)=E_L.\tag{2.6}$$

We note that the equilibrium relations (2.6) allow one to directly compute two dependent variables: h_L^* satisfies the following cubic equation:

$$(h_L^*)^3+\frac{1}{g}(gB_R-E_L)(h_L^*)^2+\frac{q_L^2}{2g}=0,\tag{2.7}$$

whose solution is discussed in Section 4 below. The remaining two unknowns can now be computed from (2.4) and (2.5), which result in

$$\begin{aligned} h_R^* &= \frac{1}{\lambda_R-\lambda_L}\Big(\lambda_R h_R-\lambda_L h_L^*-(q_R-q_L)\Big), \\ q_R^* &= \frac{1}{\lambda_R-\lambda_L}\left(\lambda_R q_R-\lambda_L q_L-\left(h_R u_R^2+\frac{g}{2}h_R^2-h_L u_L^2-\frac{g}{2}h_L^2\right)-\overline{ghB_x}\right). \end{aligned} \tag{2.8}$$

Remark 2.1. In the case when $\lambda_L<0$ and $\lambda_R<0$, the values of h_L^*, h_R^*, q_L^* and q_R^* are obtained in a similar manner:

$$q_R^*=q_R,$$

h_R^* is a solution of the cubic equation

$$(h_R^*)^3+\frac{1}{g}(gB_L-E_R)(h_R^*)^2+\frac{q_R^2}{2g}=0,$$

and then h_L^* and q_L^* are

$$\begin{aligned} h_L^* &= \frac{1}{\lambda_R-\lambda_L}\Big(\lambda_R h_R^*-\lambda_L h_L-(q_R-q_L)\Big), \\ q_L^* &= \frac{1}{\lambda_R-\lambda_L}\left(\lambda_R q_R-\lambda_L q_L-\left(h_R u_R^2+\frac{g}{2}h_R^2-h_L u_L^2-\frac{g}{2}h_L^2\right)-\overline{ghB_x}\right). \end{aligned}$$

2.2 Subcritical case

In the subcritical case, we seek an approximate solution of the Riemann problem (1.1) and (2.1) in a different form (compare with (2.2)):

$$\boldsymbol{\mathcal{W}}_{\text{sub}}(x,t)=\begin{cases} \boldsymbol{w}_L, & \text{if} \quad \frac{x}{t}<\lambda_L, \\ \boldsymbol{w}_L^*, & \text{if} \quad \lambda_L<\frac{x}{t}<0, \\ \boldsymbol{w}_R^*, & \text{if} \quad 0<\frac{x}{t}<\lambda_R, \\ \boldsymbol{w}_R, & \text{if} \quad \lambda_R<\frac{x}{t}. \end{cases} \tag{2.9}$$

As before, the bottom topography equation $B_t=0$ is trivial, which implies $B_L^*=B_L$ and $B_R^*=B_R$ and thus one has to determine h_L^*, h_R^*, q_L^* and q_R^* only; see Fig. 2, where the function $\boldsymbol{\mathcal{W}}_{\text{sub}}(x,t)$ is schematically presented in the (x,t)-plane on the rectangle $[-\frac{\Delta x}{2},\frac{\Delta x}{2}]\times[0,\Delta t]$.

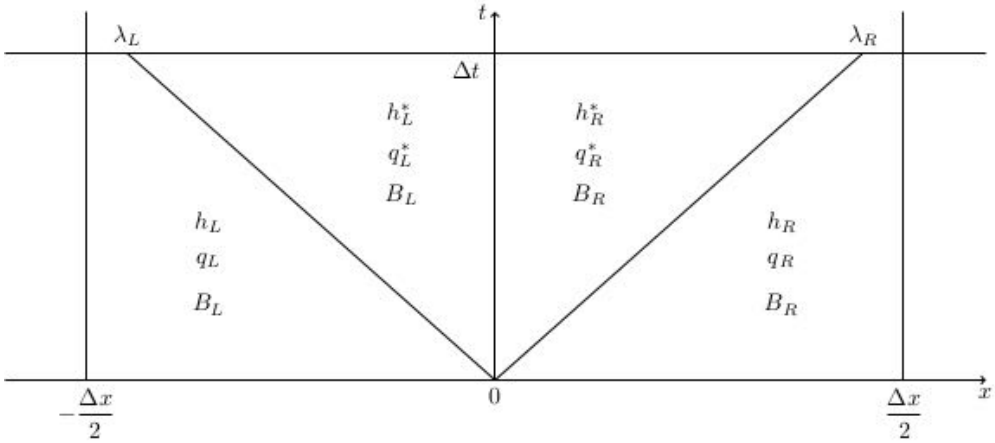

Figure 2: Structure of the HLL-type approximate Riemann problem solver $\mathcal{W}_{\text{sub}}(x,t)$.

We again use the consistency relation (2.3), this time with $\mathcal{W}=\mathcal{W}_{\text{sub}}$, which gives

$$\begin{aligned}
&\left(\frac{1}{2}+\lambda_L\mu\right)h_L-\lambda_L\mu h_L^*+\lambda_R\mu h_R^*+\left(\frac{1}{2}-\lambda_R\mu\right)h_R\\
=&\frac{1}{2}(h_L+h_R)-\mu(q_R-q_L), \qquad (2.10)\\
&\left(\frac{1}{2}+\lambda_L\mu\right)q_L-\lambda_L\mu q_L^*+\lambda_R\mu q_R^*+\left(\frac{1}{2}-\lambda_R\mu\right)q_R\\
=&\frac{1}{2}(q_L+q_R)-\mu\left(h_Ru_R^2+\frac{g}{2}h_R^2-h_Lu_L^2-\frac{g}{2}h_L^2\right)-\mu\overline{ghB_x}. \qquad (2.11)
\end{aligned}$$

Since (2.10) and (2.11) again give only two nonlinear algebraic equations for the four unknowns, additional relations have to be imposed. As in the supercritical case, we impose the equilibrium conditions across the stationary λ_0-wave:

$$q_L^*=q_R^*, \qquad (2.12)$$

$$\frac{1}{2}\left(\frac{q_L^*}{h_L^*}\right)^2+g(h_L^*+B_L)=\frac{1}{2}\left(\frac{q_R^*}{h_R^*}\right)^2+g(h_R^*+B_R). \qquad (2.13)$$

We now need to solve the system (2.10)-(2.13). First, we note that equations (2.11) and (2.12) give

$$\begin{aligned}
&q_L^*=q_R^*\\
=&q^*:=\frac{1}{\lambda_R-\lambda_L}\left(\lambda_Rq_R-\lambda_Lq_L-\left(h_Ru_R^2+\frac{g}{2}h_R^2-h_Lu_L^2-\frac{g}{2}h_L^2\right)-\overline{ghB_x}\right). \qquad (2.14)
\end{aligned}$$

We then observe that Eq. (2.13) is nonlinear and if we use it then this will result in a quintic equation, solving which will make the resulting scheme too cumbersome. We therefore replace it with

$$\frac{1}{2}\left(\frac{q^*}{\widehat{h}_L}\right)^2+g(h_L^*+B_L)=\frac{1}{2}\left(\frac{q^*}{\widehat{h}_R}\right)^2+g(h_R^*+B_R), \tag{2.15}$$

so that the system (2.10)-(2.12) and (2.15) becomes a linear algebraic system for the unknowns h_L^*, h_R^*, q_L^* and q_R^*. In (2.15), $\widehat{h}_L$ and $\widehat{h}_R$ are the averaged quantities defined as follows. We first average the energies and introduce $\widehat{E}:=\frac{1}{2}(E_L+E_R)$ and then compute $\widehat{h}_L$ and $\widehat{h}_R$ as the roots of

$$h^3+\frac{gB_L-\widehat{E}}{g}h^2+\frac{(q^*)^2}{2g}=0,\quad h^3+\frac{gB_R-\widehat{E}}{g}h^2+\frac{(q^*)^2}{2g}=0, \tag{2.16}$$

respectively. Finally, we solve (2.10) and (2.15) to find

$$\begin{aligned} h_L^*&=\frac{1}{\lambda_R-\lambda_L}(\lambda_R h_R-\lambda_L h_L-\lambda_R D+q_L-q_R),\\ h_R^*&=\frac{1}{\lambda_R-\lambda_L}(\lambda_R h_R-\lambda_L h_L-\lambda_L D+q_L-q_R), \end{aligned} \tag{2.17}$$

where

$$D:=\frac{(q^*)^2}{2g}\left(\frac{1}{\widehat{h}_L^2}-\frac{1}{\widehat{h}_R^2}\right)+(B_L-B_R). \tag{2.18}$$

Remark 2.2. Notice that if $B_L=B_R$, then (2.16) implies $\widehat{h}_L=\widehat{h}_R$, (2.18), in turn, implies $D=0$, and thus we obtain from (2.17) that

$$h_L^*=h_R^*=\frac{1}{\lambda_R-\lambda_L}(\lambda_R h_R-\lambda_L h_L+q_L-q_R).$$

2.3 Critical case

Finally, we consider the critical case, in which either λ_L or λ_R vanishes. Let us assume that $\lambda_L=0$ (the case $\lambda_R=0$ is treated similarly) and seek an approximate solution of the Riemann problem (1.1) and (2.1) in the following form, which is simpler that either (2.2) or (2.9):

$$\mathcal{W}_{\rm cr}(x,t)=\begin{cases} \boldsymbol{w}_L, & \text{if} \quad \frac{x}{t}<0,\\ \boldsymbol{w}^*, & \text{if} \quad 0<\frac{x}{t}<\lambda_R,\\ \boldsymbol{w}_R, & \text{if} \quad \lambda_R<\frac{x}{t}. \end{cases}$$

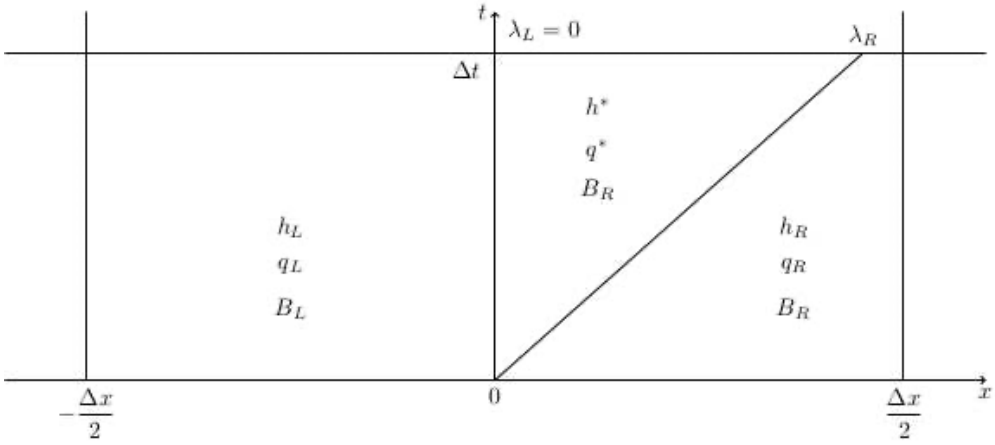

Figure 3: Structure of the HLL-type approximate Riemann problem solver $\mathcal{W}_{\rm cr}(x,t)$.

As in the previous two cases, $B_t=0$ implies $B^*=B_R*$ and one has to determine two unknowns h^* and q^* only; see Fig. 3, where the function $\mathcal{W}_{\rm cr}(x,t)$ is schematically presented in the (x,t)-plane on the rectangle $[-\frac{\Delta x}{2},\frac{\Delta x}{2}]\times[0,\Delta t]$.

In the critical case, we simply use the consistency relation (2.3) with $\mathcal{W}=\mathcal{W}_{\rm cr}$ and obtain

$$\begin{aligned} h^* &= h_R - \frac{1}{\lambda_R}(q_R - q_L), \\ q^* &= q_R - \frac{1}{\lambda_R}\left(h_R u_R^2 + \frac{g}{2}h_R^2 - h_L u_L^2 - \frac{g}{2}h_L^2 + \overline{ghB_x}\right). \end{aligned} \tag{2.19}$$

Remark 2.3. In the case when $\lambda_L < 0$ and $\lambda_R = 0$, the values of h_* and q_R are obtained in a similar manner:

$$\begin{aligned} h^* &= h_L + \frac{1}{\lambda_L}(q_R - q_L), \\ q^* &= q_L + \frac{1}{\lambda_L}\left(h_R u_R^2 + \frac{g}{2}h_R^2 - h_L u_L^2 - \frac{g}{2}h_L^2 + \overline{ghB_x}\right). \end{aligned}$$

3 Well-balanced HLL-type schemes

In this section, we use the approximate Riemann problem solver developed in Section 2 to design well-balanced HLL-type schemes for the Saint-Venant system (1.1).

3.1 First-order scheme

We begin with the derivation of the first-order scheme.

For the sake of simplicity, we introduce uniform finite-volume cells

$$C_j=\left[x_{j-\frac{1}{2}},x_{j+\frac{1}{2}}\right]$$

of size $\Delta x:=x_{j+\frac{1}{2}}-x_{j-\frac{1}{2}}$ centered at $x_j=\frac{1}{2}(x_{j-\frac{1}{2}}+x_{j+\frac{1}{2}})$. We assume that at a certain time level $t=t^n$, the computed quantities (solution cell averages),

$$\overline{\boldsymbol{w}}_j^n\approx\frac{1}{\Delta x}\int\limits_{C_j}\boldsymbol{w}(x,t^n)\mathrm{d}x$$

are available. They are then evolved in time in the finite-volume fully discrete framework

$$\overline{\boldsymbol{w}}_j^{n+1}=\overline{\boldsymbol{w}}_j^n-\mu\left(\boldsymbol{\mathcal{F}}_{j+\frac{1}{2}}^-\boldsymbol{-}\boldsymbol{\mathcal{F}}_{j-\frac{1}{2}}^+\right),\tag{3.1}$$

where, as before, $\mu:=\frac{\Delta t}{\Delta x}$ and $\boldsymbol{\mathcal{F}}_{j\pm\frac{1}{2}}^{\mp}$ are numerical fluxes derived by the HLL-type approximate Riemann problem solver developed in Section 2.

In order to design the HLL-type numerical fluxes, we first rewrite the Saint-Venant system (1.1) in the vector form,

$$\begin{aligned}&\boldsymbol{w}_t+\boldsymbol{f}(\boldsymbol{w})_x=\boldsymbol{s}(\boldsymbol{w}),\qquad \boldsymbol{w}=\begin{pmatrix}h\\q\\B\end{pmatrix},\\&\boldsymbol{f}(\boldsymbol{w}):=\begin{pmatrix}q\\\frac{q^2}{h}+\frac{g}{2}h^2\\0\end{pmatrix},\quad \boldsymbol{s}(\boldsymbol{w}):=\begin{pmatrix}0\\-ghB_x\\0\end{pmatrix},\end{aligned}\tag{3.2}$$

and consider the Riemann problems localized at the cell interfaces: (3.2) subject to the following initial data

$$\boldsymbol{w}(x,t^n)=\begin{cases}\boldsymbol{w}_L:=\overline{\boldsymbol{w}}_j^n, & x<x_{j+\frac{1}{2}},\\ \boldsymbol{w}_R:=\overline{\boldsymbol{w}}_{j+1}^n, & x>x_{j+\frac{1}{2}},\end{cases}$$

prescribed at time level $t=t^n$. Its approximate solution is given by either $\boldsymbol{\mathcal{W}}_{\text{sup}}(x-x_{j+\frac{1}{2}},t-t^n)$, $\boldsymbol{\mathcal{W}}_{\text{sub}}(x-x_{j+\frac{1}{2}},t-t^n)$ or $\boldsymbol{\mathcal{W}}_{\text{cr}}(x-x_{j+\frac{1}{2}},t-t^n)$ as explained in Section 2.

We then follow [29] and define the numerical fluxes by applying the Rankine-Hugoniot relations across the discontinuities in the approximate Riemann problem solver. In the supercritical case, the numerical fluxes are given by either

$$\begin{cases} \mathcal{F}^-_{j+\frac{1}{2}} = \boldsymbol{f}(\boldsymbol{w}_L), \\ \mathcal{F}^+_{j+\frac{1}{2}} = \boldsymbol{f}(\boldsymbol{w}_R) - \lambda_R(\boldsymbol{w}_R - \boldsymbol{w}^*_R) - \lambda_L(\boldsymbol{w}^*_R - \boldsymbol{w}^*_L), \end{cases} \tag{3.3}$$

or

$$\begin{cases} \mathcal{F}^-_{j+\frac{1}{2}} = \boldsymbol{f}(\boldsymbol{w}_L) + \lambda_L(\boldsymbol{w}^*_L - \boldsymbol{w}_L) + \lambda_R(\boldsymbol{w}^*_R - \boldsymbol{w}^*_L), \\ \mathcal{F}^+_{j+\frac{1}{2}} = \boldsymbol{f}(\boldsymbol{w}_R), \end{cases} \tag{3.4}$$

depending on whether $\lambda_R > \lambda_L > 0$ or $\lambda_L < \lambda_R < 0$, respectively. The intermediate values $\boldsymbol{w}^*_L$ and $\boldsymbol{w}^*_R$ are computed in Section 2.1. In the subcritical case, the numerical fluxes are

$$\begin{cases} \mathcal{F}^-_{j+\frac{1}{2}} = \boldsymbol{f}(\boldsymbol{w}_L) + \lambda_L(\boldsymbol{w}^*_L - \boldsymbol{w}_L), \\ \mathcal{F}^+_{j+\frac{1}{2}} = \boldsymbol{f}(\boldsymbol{w}_R) - \lambda_R(\boldsymbol{w}_R - \boldsymbol{w}^*_R) \end{cases} \tag{3.5}$$

with $\boldsymbol{w}^*_L$ and $\boldsymbol{w}^*_R$ computed in Section 2.2. Finally, in the critical case, the numerical fluxes are given by either

$$\begin{cases} \mathcal{F}^-_{j+\frac{1}{2}} = \boldsymbol{f}(\boldsymbol{w}_L), \\ \mathcal{F}^+_{j+\frac{1}{2}} = \boldsymbol{f}(\boldsymbol{w}_R) - \lambda_R(\boldsymbol{w}_R - \boldsymbol{w}^*), \end{cases} \tag{3.6}$$

or

$$\begin{cases} \mathcal{F}^-_{j+\frac{1}{2}} = \boldsymbol{f}(\boldsymbol{w}_L) + \lambda_L(\boldsymbol{w}^* - \boldsymbol{w}_L), \\ \mathcal{F}^+_{j+\frac{1}{2}} = \boldsymbol{f}(\boldsymbol{w}_R), \end{cases} \tag{3.7}$$

depending on whether $\lambda_R > \lambda_L = 0$ or $\lambda_L < \lambda_R = 0$, respectively. The intermediate values $\boldsymbol{w}^*$ are computed in Section 2.3.

Remark 3.1. We note that if $\overline{B}_j = \overline{B}_{j+1}$, then $\mathcal{F}^-_{j+\frac{1}{2}} = \mathcal{F}^+_{j+\frac{1}{2}}$ as expected since in this case, the system of balance laws (3.2) is locally conservative at $x = x_{j+\frac{1}{2}}$.

3.1.1 Well-balanced source discretization

In order to complete the derivation of the well-balanced HLL-type scheme, we need to make sure that if the approximate solution at time $t = t^n$ is at (moving-water) equilibrium (1.2), that is, if there exist two constants $\mathcal{Q}$ and $\mathcal{E}$ such that

$$\overline{q}^n_j = \overline{q}^n_{j+1} = \mathcal{Q}, \quad \frac{1}{2}\left(\frac{\overline{q}^n_j}{\overline{h}^n_j}\right)^2 + g\left(\overline{h}^n_j + \overline{B}_j\right) = \frac{1}{2}\left(\frac{\overline{q}^n_{j+1}}{\overline{h}^n_{j+1}}\right)^2 + g\left(\overline{h}^n_{j+1} + \overline{B}_{j+1}\right) = \mathcal{E} \tag{3.8}$$

for all j, then the intermediate values would satisfy

$$\begin{aligned}
&\boldsymbol{w}_L^* = \boldsymbol{w}_R^* = \boldsymbol{w}_R && \text{in the supercritical case with } 0<\lambda_L<\lambda_R, && (3.9)\\
&\boldsymbol{w}_L^* = \boldsymbol{w}_R^* = \boldsymbol{w}_L && \text{in the supercritical case with } \lambda_L<\lambda_R<0, && (3.10)\\
&\boldsymbol{w}_L^* = \boldsymbol{w}_L,\ \boldsymbol{w}_R^* = \boldsymbol{w}_R && \text{in the subcritical case,} && (3.11)\\
&\boldsymbol{w}^* = \boldsymbol{w}_R && \text{in the critical case with } 0=\lambda_L<\lambda_R, && (3.12)\\
&\boldsymbol{w}^* = \boldsymbol{w}_L && \text{in the critical case with } \lambda_L<\lambda_R=0. && (3.13)
\end{aligned}$$

This will imply that $\boldsymbol{\mathcal{F}}^-_{j+\frac{1}{2}} = \boldsymbol{\mathcal{F}}^+_{j-\frac{1}{2}}$ and hence

$$\overline{\boldsymbol{w}}_j^{n+1} = \overline{\boldsymbol{w}}_j^n - \mu\left(\boldsymbol{\mathcal{F}}^-_{j+\frac{1}{2}} - \boldsymbol{\mathcal{F}}^+_{j-\frac{1}{2}}\right) = \overline{\boldsymbol{w}}_j^n,$$

which means that the approximate solution at time $t=t^{n+1}$ will stay at the steady state.

Theorem 3.1. *If the approximate solution at time $t=t^n$ satisfies* (3.8) *and the following source discretization,*

$$\overline{ghB_x} = \frac{g}{2}(B_R-B_L)(h_R+h_L) - \frac{h_R-h_L}{4}(u_R-u_L)^2 \tag{3.14}$$

is utilized in the approximate Riemann problem solver presented in Section 2*, then* (3.9)-(3.13) *are satisfied and the resulting first-order HLL-type scheme* (3.1) *and* (3.3)-(3.7) *is well-balanced.*

Proof. We consider the three possible cases: (i) supercritical, (ii) subcritical and (iii) critical.

(i) For the sake of simplicity, we will only consider the case when $\lambda_R>\lambda_L>0$ (the other supercritical case when $\lambda_L<\lambda_R<0$ is treated similarly). In this case, we first use (2.6) and (3.8) to obtain $h_L^* = \overline{h}^n_{j+1}$ and $q_L^* = \mathcal{Q}$. Next, we substitute this into (3.14) and then into (2.8) to obtain $h_R^* = \overline{h}^n_{j+1}$ and $q_R^* = \mathcal{Q}$. Thus, (3.9) is satisfied.

(ii) In this case, we first use (2.14), (3.8) and (3.14) to obtain $q_L^* = q_R^* = \mathcal{Q}$, which are then substituted into (2.18), which together with the second equation in (3.8) gives $D = h_R - h_L$. This, in turn, is substituted into (2.17) to obtain $h_L^* = h_L$ and $h_R^* = h_R$ and hence (3.11) is satisfied.

(iii) Finally, in the critical case we will only consider the case when $\lambda_R > \lambda_L = 0$ (the other critical case when $\lambda_L < \lambda_R = 0$ is treated similarly). In this case, we substitute (3.8) and (3.14) into (2.19), which results in (3.12).

□

Remark 3.2. For the still-water equilibria (1.3), the source discretization (3.14) reduces to

$$\overline{ghB_x} = \frac{g}{2}(B_R - B_L)(h_R + h_L),$$

which has been used in a variety Godunov-type schemes (see, e.g., [1, 20]) to ensure still-water equilibria preserving property.

Remark 3.3. The source discretization (3.14) is the same as one used in [27] and [10] in the context of WENO and central-upwind schemes, respectively, as well as several other moving-water equilibria preserving methods. We note that in the case of flat bottom topography, (3.14) is inconsistent as its right-hand side (RHS) does not vanish. In the case of a smooth solution, the first term in the RHS of (3.14) is an approximation of $-ghb_x$, while the last term on the RHS of (3.14) is proportional to $(\Delta x)^3$ so that the size of the local truncation error of the resulting HLL-type scheme is not significantly affected (this is also true for the second-order HLL-type scheme presented in Section 3.2 below). However, if the solution is nonsmooth, which is a generic case for the nonlinear hyperbolic system (1.1), then the lack of consistency may become more transparent. A way to cure this defect is subject of future study and is beyond the scope of this paper.

3.2 Second-order scheme

We now extend the designed HLL-type scheme to the second order of accuracy. The extension is carried out using the semi-discrete approach. We assume that at a certain time level t the solution, realized in terms of its cell averages,

$$\overline{\boldsymbol{w}}_j(t) \approx \frac{1}{\Delta x}\int\limits_{C_j} \boldsymbol{w}(x,t)\,\mathrm{d}x$$

is available. They are then evolved in time by solving the system of ODEs,

$$\frac{\mathrm{d}}{\mathrm{d}t}\overline{\boldsymbol{w}}_j(t) = -\frac{1}{\Delta x}\left(\boldsymbol{\mathcal{F}}^-_{j+\frac{1}{2}}(t) - \boldsymbol{\mathcal{F}}^+_{j-\frac{1}{2}}(t)\right), \tag{3.15}$$

where the numerical fluxes are still given by (3.3)-(3.7), but the values of $\boldsymbol{w}_L$ and $\boldsymbol{w}_R$ at the cell interface $x=x_{j+\frac{1}{2}}$ are now computed using a piecewise linear reconstruction as described below.

We follow the approach from [34] (also see [10,33]) and reconstruct the equilibrium variables (E and q) rather than the conservative ones (h and q). We first compute

$$E_j := \frac{1}{2}\left(\frac{\overline{q}_j^n}{\overline{h}_j^n}\right)^2 + g\left(\overline{h}_j^n + \overline{B}_j\right) \quad \text{for all } j, \tag{3.16}$$

and then use the generalized minmod limiter [23,25,30] to evaluate the numerical derivatives

$$(E_x)_j = \text{minmod}\left(\theta\frac{\overline{E}_{j+1}-\overline{E}_j}{\Delta x}, \frac{\overline{E}_{j+1}-\overline{E}_{j-1}}{2\Delta x}\theta\frac{\overline{E}_j-\overline{E}_{j-1}}{\Delta x}\right), \tag{3.17}$$

$$(q_x)_j = \text{minmod}\left(\theta\frac{\overline{q}_{j+1}-\overline{q}_j}{\Delta x}, \frac{\overline{q}_{j+1}-\overline{q}_{j-1}}{2\Delta x}, \theta\frac{\overline{q}_j-\overline{q}_{j-1}}{\Delta x}\right), \tag{3.18}$$

where $\theta\in[1,2]$ is a parameter helps to control the smoothness of the reconstructed values (larger values of θ correspond to sharper, but more oscillatory reconstructions) and the minmod function is defined as

$$\text{minmod}(\alpha,\beta,\gamma) = \frac{1}{2}\big(\text{sgn}(\alpha)+\text{sgn}(\gamma)\big)\min\big(|\alpha|,|\beta|,|\gamma|\big).$$

The reconstructed point values of E and q are then

$$E_L = E_j + \frac{\Delta x}{2}(E_x)_j, \quad E_R = E_{j+1} - \frac{\Delta x}{2}(E_x)_{j+1},$$
$$q_L = \overline{q}_j + \frac{\Delta x}{2}(q_x)_j, \quad q_R = \overline{q}_{j+1} - \frac{\Delta x}{2}(q_x)_{j+1}.$$

As in [34], the bottom topography is not reconstructed since

$$\frac{1}{\Delta x}\left(\overline{B}_{j+1}-\overline{B}_j\right) = B_x\left(x_{j+\frac{1}{2}}\right) + \mathcal{O}\left((\Delta x)^2\right)$$

as long as B is sufficiently smooth. Finally, the required point values h_L and h_R are obtained by solving the corresponding cubic equations,

$$h_L^3 + \frac{1}{g}\left(g\overline{B}_j - E_L\right)h_L^2 + \frac{q_L^2}{2g} = 0, \quad h_R^3 + \frac{1}{g}\left(g\overline{B}_{j+1} - E_R\right)h_R^2 + \frac{q_R^2}{2g} = 0, \tag{3.19}$$

whose solution is discussed in Section 4 below.

Remark 3.4. If there are two physically relevant solutions of some of the cubic equations in (3.19), we choose h_L and h_R in the same flow regime as the cell centered values in cells C_j and C_{j+1}, respectively, as suggested in [33]. If some of the cubic equations in (3.19) have no positive real solutions, we then set

$$h_L=\left(\frac{q_L^2}{g}\right)^{\frac{1}{3}} \quad \text{or} \quad h_R=\left(\frac{q_R^2}{g}\right)^{\frac{1}{3}},$$

respectively, which corresponds to the critical flow regime as explained in Section 4 below.

Remark 3.5. Notice that at the moving-water equilibria, the equilibrium variables E and q are constant and hence the slopes in (3.18) are 0 and all of the interface values will coincide with the corresponding cell centered values. Therefore, the resulting second-order semi-discrete scheme (3.15) and (3.3)-(3.7) will be well-balanced as the proof of Theorem 3.1 is still valid.

Remark 3.6. The system of ODEs (3.15) has to be solved using a sufficiently stable and accurate ODE solver. In the numerical examples reported in Section 5, we have use the three-stage third-order strong stability preserving (SSP) Runge-Kutta solver; see, e.g., [14, 15].

4 Variable transformation

In this section, we describe the way to solve Eqs. (2.7) for h_L and (3.19) for h_L and h_R, that is, we show how one can switch from the equilibrium variables q, E and B to the conservative variables h, q and B. To this end, we need to solve the following cubic equation:

$$P(h):=h^3+a_0h^2+a_2=0, \tag{4.1}$$

where

$$a_0:=\frac{1}{g}(gB-E), \quad a_2:=\frac{q^2}{2g}.$$

We note that $a_2\geq 0$ and from the definition of E in (1.2), $a_0<0$ as long as $h>0$ (in this paper we do not consider the case of dry areas).

One can easily show that:

- the polynomial P has either one or three real roots;

- the limits at infinities are $\lim_{h\to\pm\infty} P(h)=\pm\infty$;
- P attains a local maximum at $\widetilde{h}_1=0$ and a local minimum at $\widetilde{h}_2=-\frac{2a_0}{3}>0$;
- P has a nonphysical negative root $\bar{h}_1<0$;
- Since $P(0)>0$, P has at least one positive root if $P(\widetilde{h}_2)\geq 0 \Longleftrightarrow a_2\leq -\frac{4}{27}a_0^3$;
- Depending on the value of a_2, we can distinguish between the following three physically relevant cases:

$$\begin{cases} a_2=0 & \to \quad \text{fluid at rest,} \\ 0<a_2<-\frac{4}{27}a_0^3 & \to \quad \text{sub/supercritical flow,} \\ a_2=-\frac{4}{27}a_0^3 & \to \quad \text{critical flow.} \end{cases}$$

Fluid at Rest. In this case, the unique physically relevant double root is $\bar{h}_2=\bar{h}_3=-a_0$.

Critical Flow. In this case, the unique physically relevant double root is $\bar{h}_2=\bar{h}_3=-\frac{2a_0}{3}$.

Sub/Supercritical Flow. In this case, there are two physically relevant roots: the supercritical ($\bar{h}_2<\widetilde{h}_2$) and subcritical ($\bar{h}_3>\widetilde{h}_2$) ones. In order to find these roots, we make the substitution $h=t-\frac{a_0}{3}$ and rewrite Eq. (4.1) in the following depressed form:

$$Q(t):=t^3-\frac{a_0^2}{3}t+\frac{27a_2+2a_0^3}{27}=0.$$

According to [22], the roots of Q can be written in the following explicit form:

$$\bar{t}_i=-\frac{2}{3}a_0\cos\left(\frac{\phi+2\pi i}{3}\right), \quad i=1,2,3,$$

where $\phi\in(0,\pi)$ such that

$$\cos\phi=1+\frac{27a_2}{2a_0^3}.$$

Thus, the corresponding roots of P are

$$\bar{h}_i=-\frac{1}{3}a_0\left[2\cos\left(\frac{\phi+2\pi i}{3}\right)+1\right], \quad i=1,2,3. \tag{4.2}$$

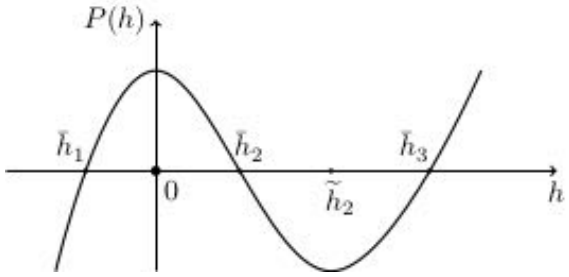

Figure 4: Roots of $P(h)$ in the sub/supercritical flow case.

It is straightforward to check that

$$\bar{h}_1 < 0 < \bar{h}_2 < \widetilde{h}_2 < \bar{h}_3,$$

which means that the three roots in (4.2) are nonphysical ($\bar{h}_1$), supercritical ($\bar{h}_2$) and subcritical ($\bar{h}_3$), respectively; see Fig. 4.

5 Numerical examples

In this section, we demonstrate the performance of the developed second-order HLL-type numerical scheme. Since the scheme is derived for different flow regimes, we use the following set of equilibria as a basis for our numerical experiments:

$$\text{Subcritical flow:} \quad q_{\text{eq}} = 4.42, \quad E_{\text{eq}} = 22.06605, \tag{5.1}$$

$$\text{Transcritical flow:} \quad q_{\text{eq}} = 1.53, \quad E_{\text{eq}} = 11.090714039778195, \tag{5.2}$$

$$\text{Supercritical flow:} \quad q_{\text{eq}} = 24, \quad E_{\text{eq}} = 91.624. \tag{5.3}$$

We consider either continuous,

$$B(x) = \begin{cases} 0.2 - 0.05(x-10)^2, & \text{if} \quad 8 \le x \le 12, \\ 0, & \text{otherwise}, \end{cases} \tag{5.4}$$

or discontinuous,

$$B(x) = \begin{cases} 0.2, & \text{if} \quad 8 \le x \le 12, \\ 0, & \text{otherwise}, \end{cases} \tag{5.5}$$

bottom topographies.

In all of the numerical examples, we take the acceleration due to gravity $g = 9.812$, the minmod parameter $\theta = 1.3$, the CFL number 0.5, and use uniform finite-volume meshes on the computational domain $[0,25]$.

Example 5.1 (**Moving-water equilibria preserving well-balanced test).** In the first example, we consider the initial data, given in terms of the equilibrium variables q and E:

$$q(x,0)\equiv q_{\text{eq}},\quad E(x,0)\equiv E_{\text{eq}},$$

where q_{eq} and E_{eq} are given by one of the equilibrium states (5.1), (5.2) or (5.3). We notice that the initial data given by (5.1)-(5.3) are in terms of the equilibrium variables q and E instead of the original conservative variables q and h. However, in order to initiate the computations at time $t=0$, the values of $\overline{h}_j(0)$ are required. They can be obtained by solving the nonlinear algebraic equation (3.16) as described in Section 4. It should be pointed out that in the transcritical flow case (5.2), the shape of the bottom topography will influence the solution procedure. In order to single out the unique solution, we refer to [10, Remark 4.1]. In particular, if B is the continuous function given by (5.4), then the flow is

$$\begin{cases}\text{subcritical}, & \text{if} \quad x_j<10,\\ \text{supercritical}, & \text{if} \quad x_j>10,\end{cases} \tag{5.6}$$

and if B is the discontinuous function given by (5.5), then the flow is

$$\begin{cases}\text{subcritical}, & \text{if} \quad x_j<8,\\ \text{critical}, & \text{if} \quad 8\le x_j\le 12,\\ \text{supercritical}, & \text{if} \quad x_j>12.\end{cases} \tag{5.7}$$

We use two different bottom topographies, (5.4) and (5.5), and compute the numerical solution of the resulting six initial value problems until the final time $t=20$ by the HLL-type scheme using 200 cells. In order to test the well-balanced property of the studied schemes, we measure the L^1-error of the computed solutions and report the obtained results in Table 1. These results demonstrate that the HLL-type scheme preserves the moving-water equilibria within the machine

Table 1: Example 5.1: L^1-errors in h, q and E for the HLL-type scheme in three different flow regimes with two different bottom topographies.

	$\|h(\cdot,20)-h_{\text{eq}}\|_1$			$\|q(\cdot,20)-q_{\text{eq}}\|_1$			$\|E(\cdot,20)-E_{\text{eq}}\|_1$		
$B(x)$ \ q_{eq}, E_{eq}	(5.1)	(5.2)	(5.3)	(5.1)	(5.2)	(5.3)	(5.1)	(5.2)	(5.3)
(5.4)	4.99E-16	6.94E-17	8.29E-14	1.55E-15	3.91E-15	5.83E-13	8.44E-15	4.55E-14	3.86E-12
(5.5)	5.55E-17	<1.0E-17	5.23E-14	1.11E-16	<1.0E-17	6.57E-13	4.44E-16	3.06E-14	2.14E-12

error in all of the cases. This verifies the desired well-balanced property of the proposed scheme.

Example 5.2 (**Convergence to moving-water equilibria).** In this example, we consider the following four initial-boundary value problems with the "lake at rest" initial conditions and the boundary conditions that correspond to the equilibria defined in (5.1)-(5.3), namely:

$$\text{Subcritical flow:} \quad \begin{cases} h(x,0)=2-B(x), & q(x,0)=0, \\ q(0,t)=4.42, & h(25,t)=2, \end{cases} \tag{5.8}$$

$$\text{Transcritical flow without a shock:} \quad \begin{cases} h(x,0)=0.66-B(x), & q(x,0)=0, \\ q(0,t)=1.53, & h(25,t)=0.66, \end{cases} \tag{5.9}$$

$$\text{Transcritical flow with a shock:} \quad \begin{cases} h(x,0)=0.33-B(x), & q(x,0)=0, \\ q(0,t)=0.18, & h(25,t)=0.33, \end{cases} \tag{5.10}$$

$$\text{Supercritical flow:} \quad \begin{cases} h(x,0)=2-B(x), & q(x,0)=0, \\ h(0,t)=2, & q(0,t)=24. \end{cases} \tag{5.11}$$

Remark 5.1. In case (5.9), the downstream boundary condition $(h(25,t)=0.66)$ is imposed only when the flow is subcritical.

We take the continuous bottom topography (5.4) and compute the numerical solutions using the HLL-type scheme until the final time $t=200$ with 200 uniform cells for all of the aforementioned four cases. In Figs. 5-8, we plot the obtained numerical results. As one can see, the water depth h obtained by the proposed HLL-type scheme are very close to the corresponding steady states in all of the four cases. One can also observe that both q and E converge to constants in cases (5.8), (5.9) and (5.11). However, Fig. 7 shows that q and E do not become flat in the transcritical case with a shock, (5.10), since the errors at the shock are $\mathcal{O}(1)$.

We now verify whether the computed solutions converge to the steady states given by (5.1)-(5.3). To this end, we measure the L^1-norm of the differences in h, q and E between the corresponding computed and steady-state solutions. In order to ensure that the discrete steady states has been reached, we run the simulation until very large final times: $T=500$ in the case (5.8) and $T=200$ in the cases (5.9) and (5.11). The obtained results are reported in Table 2. As one can clearly see, in the cases (5.8) and (5.11), the discrete steady-state solutions coincide with the steady states (5.1) and (5.3), respectively. On the other hand, in the transcritical case (5.9), the discrete and continuous steady states are slightly different; see Fig. 9.

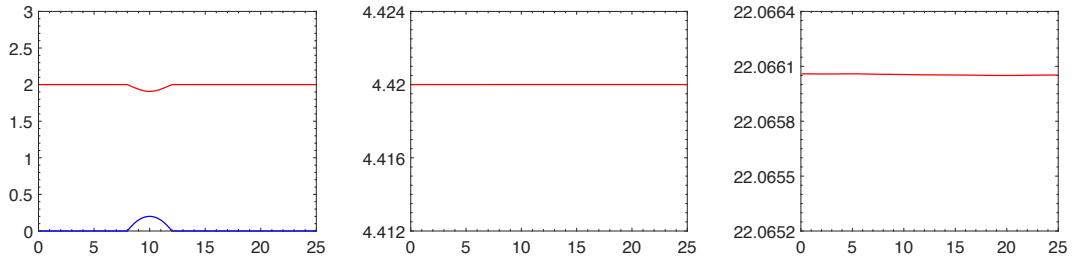

Figure 5: Example 5.2: $h+B$ (left, the blue line denotes the bottom topography $B(x)$), q (middle) and E (right), computed by the HLL-type scheme in the case (5.8).

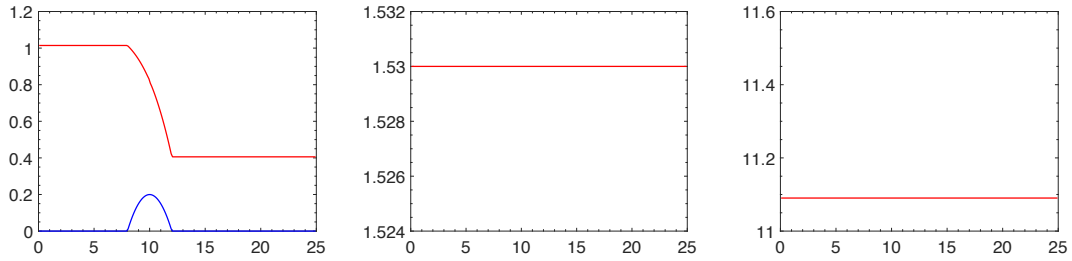

Figure 6: Example 5.2: Same as in Fig. 5, but for the case (5.9).

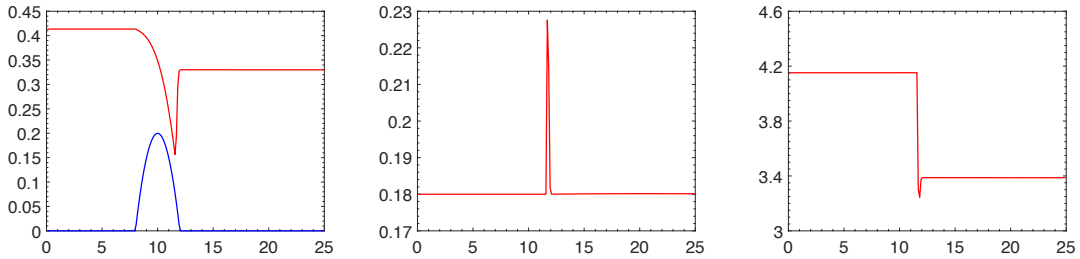

Figure 7: Example 5.2: Same as in Fig. 5, but for the case (5.10).

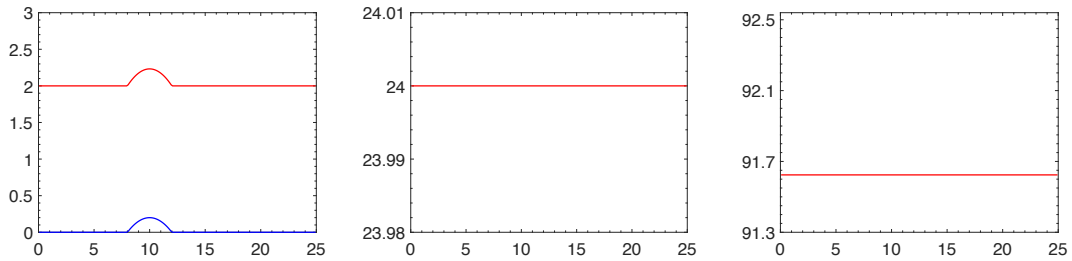

Figure 8: Example 5.2: Same as in Fig. 5, but for the case (5.11).

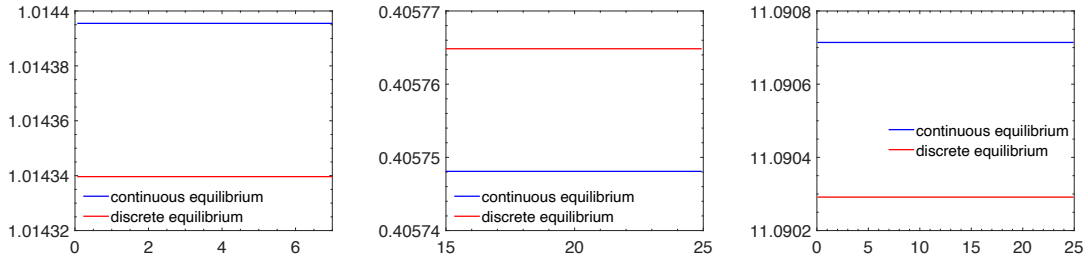

Figure 9: Example 5.2: Continuous and discrete equilibria in the transcritical case (5.9): h (zooms at $x\in[0,7]$, left, and at $x\in[15,25]$, middle) and E (right).

Table 2: Example 5.2: L^1-norm of the differences in h, q and E between the corresponding computed and steady-state solutions in three different flow regimes.

L^1-differences \ Initial data	(5.8)	(5.9)	(5.11)
$\|h(\cdot,T)-h_{\rm eq}\|_1$	4.54E-12	0.0012	6.93E-14
$\|q(\cdot,T)-q_{\rm eq}\|_1$	4.97E-12	5.17E-12	6.22E-13
$\|E(\cdot,T)-E_{\rm eq}\|_1$	2.74E-11	0.0106	4.65E-12

Example 5.3 (Small perturbations of moving-water equilibria). In the final example, we test the ability of the HLL-type scheme to capture propagation of small perturbations of moving-water equilibria. To this end, we add a small disturbance in the water depth to the equilibria (5.1)-(5.3), namely, we consider the following initial data:

$$h(x,0)=h_{\rm eq}(x)+0.05\cdot\chi_{[5.75,6.25]},\quad q(x,0)\equiv q_{\rm eq},$$

where $\chi_{[5.75,6.25]}$ is a characteristic function of the interval $[5.75,6.25]$. We consider both continuous (5.4) and discontinuous (5.5) bottom topographies. The equilibrium state $h_{\rm eq}(x)$ is represented by its cell averages, $\{\bar{h}_j(0)\}$, which are obtained precisely the same way as in Example 5.1. We note that this example was considered in [10], where it was demonstrated that a second-order central-upwind scheme that was capable of preserving the "lake at rest" (still-water) equilibria only, generated very large oscillation especially when a coarse mesh was used.

We compute the numerical solutions using the proposed HLL-type scheme until $t=1$ in the supercritical case and until $t=1.5$ in the transcritical and subcritical cases with 100 and 1000 uniform cells, respectively. In Figs. 10-12, we compare the difference between the obtained h and the background moving steady state

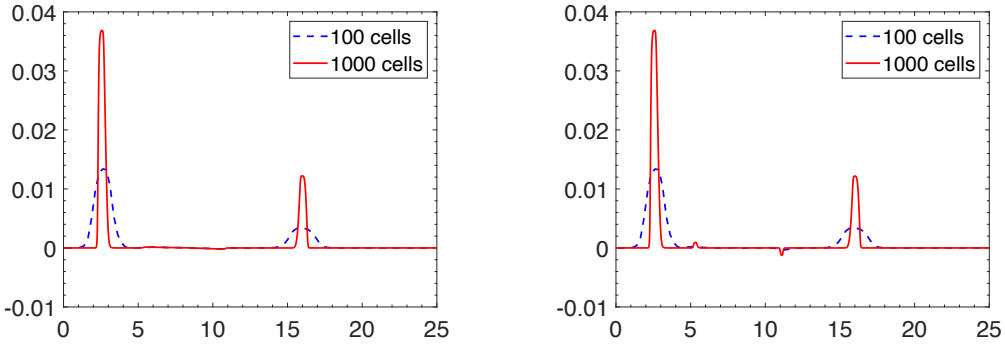

Figure 10: Example 5.3: The difference between h and the background moving steady state water depth for the subcritical flow (5.1) over the continuous (left) and discontinuous (right) bottom topographies.

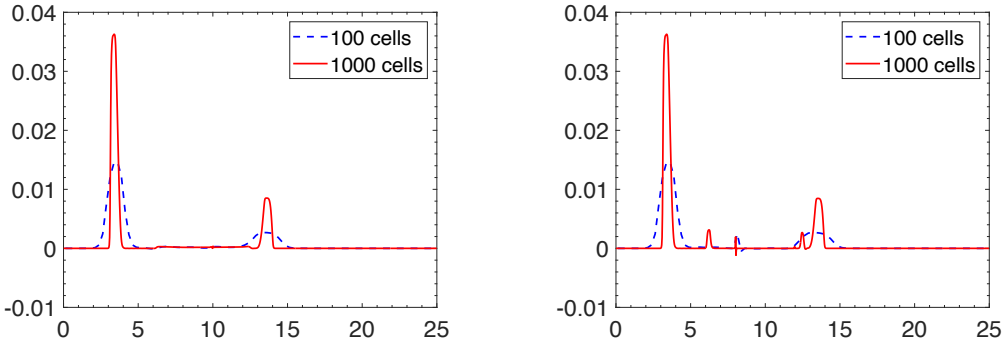

Figure 11: Example 5.3: Same as in Fig. 10, but for the transcritical flow (5.2).

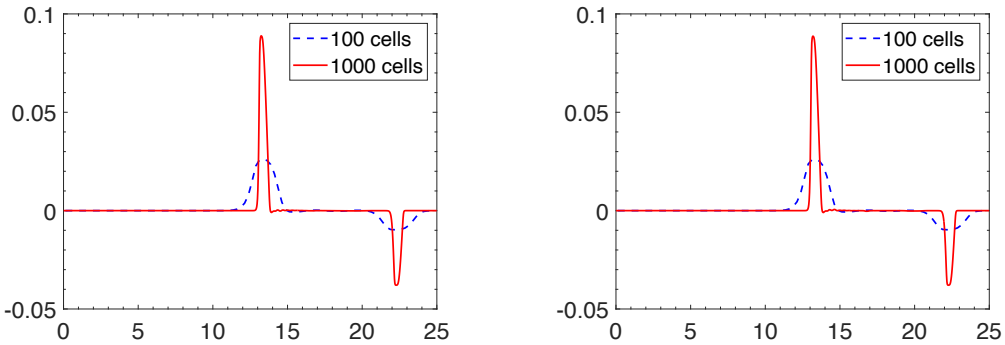

Figure 12: Example 5.3: Same as in Fig. 10, but for the supercritical flow (5.3).

water depth h_{eq}. As one can see, the obtained results are oscillation-free on both coarse and fine meshes in the continuous bottom topography case. When B is discontinuous, small spurious waves are generated over the bottom discontinuities.

However, the results obtained by the proposed scheme are of the same quality as those computed by a moving-water equilibria preserving central-upwind scheme developed in [10].

Acknowledgments

The work of A. Kurganov was supported in part by NSFC grant (No. 11771201) and by the fund of the Guangdong Provincial Key Laboratory of Computational Science and Material Design (No. 2019B030301001).

References

[1] E. Audusse, F. Bouchut, M.-O. Bristeau, R. Klein, and B. Perthame, A fast and stable well-balanced scheme with hydrostatic reconstruction for shallow water flows, SIAM J. Sci. Comput., 25 (2004), 2050-2065.

[2] A. Bermudez and M. E. Vazquez, Upwind methods for hyperbolic conservation laws with source terms, Comput. & Fluids, 23 (1994), 1049-1071.

[3] C. Berthon and C. Chalons, A fully well-balanced, positive and entropy-satisfying Godunov-type method for the shallow-water equations, Math. Comp., 85 (2016), 1281-1307.

[4] A. Bollermann, G. Chen, A. Kurganov, and S. Noelle, A well-balanced reconstruction of wet/dry fronts for the shallow water equations, J. Sci. Comput., 56 (2013), 267-290.

[5] F. Bouchut, Nonlinear Stability of Finite Volume Methods for Hyperbolic Conservation Laws and Well-Balanced Schemes for Sources, Frontiers in Mathematics, Birkhäuser Verlag , 2004.

[6] F. Bouchut and T. Morales de Luna, A subsonic-well-balanced reconstruction scheme for shallow water flows, SIAM J. Numer. Anal., 48 (2010), 1733-1758.

[7] M. Castro, J. M. Gallardo, J. A. López-Garcí a, and C. Parés, Well-balanced high order extensions of Godunov's method for semilinear balance laws, SIAM J. Numer. Anal., 46 (2008), 1012-1039.

[8] M. J. Castro, A. Pardo Milanés, and C. Parés, Well-balanced numerical schemes based on a generalized hydrostatic reconstruction technique, Math. Models Methods Appl. Sci., 17 (2007), 2055-2113.

[9] Y. Cheng, A. Chertock, M. Herty, A. Kurganov, and T. Wu, A new approach for designing moving-water equilibria preserving schemes for the shallow water equations, J. Sci. Comput., 80 (2019), 538-554.

[10] Y. Cheng and A. Kurganov, Moving-water equilibria preserving central-upwind schemes for the shallow water equations, Commun. Math. Sci., 14 (2016), 1643-1663.

[11] A. J. C. de Saint-Venant, Thèorie du mouvement non-permanent des eaux, avec application aux crues des rivière at à l'introduction des marèes dans leur lit., C.R. Acad. Sci. Paris, 73 (1871), 147-154.
[12] V. Desveaux, M. Zenk, C. Berthon, and C. Klingenberg, A well-balanced scheme for the Euler equation with a gravitational potential, in Finite volumes for complex applications VII. Methods and theoretical aspects, vol. 77 of Springer Proc. Math. Stat., Springer, Cham, 2014, 217-226.
[13] L. Gosse, A well-balanced flux-vector splitting scheme designed for hyperbolic systems of conservation laws with source terms, Comput. Math. Appl., 39 (2000), 135-159.
[14] S. Gottlieb, D. Ketcheson, and C.-W. Shu, Strong Stability Preserving Runge-Kutta and Multistep Time Discretizations, World Scientific Publishing Co. Pte. Ltd., Hackensack, 2011.
[15] S. Gottlieb, C.-W. Shu, and E. Tadmor, Strong stability-preserving high-order time discretization methods, SIAM Rev., 43 (2001), 89-112.
[16] J. M. Greenberg and A. Y. Leroux, A well-balanced scheme for the numerical processing of source terms in hyperbolic equations, SIAM J. Numer. Anal., 33 (1996), 1-16.
[17] A. Harten, P. Lax, and B. van Leer, On upstream differencing and Godunov-type schemes for hyperbolic conservation laws, SIAM Rev., 25 (1983), 35-61.
[18] S. Jin, A steady-state capturing method for hyperbolic systems with geometrical source terms, M2AN Math. Model. Numer. Anal., 35 (2001), 631-645.
[19] A. Kurganov, Finite-volume schemes for shallow-water equations, Acta Numer., 27 (2018), 289-351.
[20] A. Kurganov and D. Levy, Central-upwind schemes for the Saint-Venant system, M2AN Math. Model. Numer. Anal., 36 (2002), 397-425.
[21] A. Kurganov and G. Petrova, A second-order well-balanced positivity preserving central-upwind scheme for the Saint-Venant system, Commun. Math. Sci., 5 (2007), 133-160.
[22] W. D. Lambert, A generalized trigonometric solution of the cubic equation, Amer. Math. Monthly, 13 (1906), 73-76.
[23] K.-A. Lie and S. Noelle, On the artificial compression method for second-order nonoscillatory central difference schemes for systems of conservation laws, SIAM J. Sci. Comput., 24 (2003), 1157-1174.
[24] V. Michel-Dansac, C. Berthon, B. Clain, and F. Foucher, A well-balanced scheme for the shallow-water equations with topography, Comput. Math. Appl., 72 (2016), 568-593.
[25] H. Nessyahu and E. Tadmor, Nonoscillatory central differencing for hyperbolic conservation laws, J. Comput. Phys., 87 (1990), 408-463.
[26] S. Noelle, N. Pankratz, G. Puppo, and J. R. Natvig, Well-balanced finite volume

schemes of arbitrary order of accuracy for shallow water flows, J. Comput. Phys., 213 (2006), 474-499.

[27] S. Noelle, Y. Xing, and C.-W. Shu, High-order well-balanced finite volume WENO schemes for shallow water equation with moving water, J. Comput. Phys., 226 (2007), 29-58.

[28] C. Parés and M. Castro, On the well-balance property of Roe's method for nonconservative hyperbolic systems. Applications to shallow-water systems, M2AN Math. Model. Numer. Anal., 38 (2004), 821-852.

[29] E. F. Toro, Riemann Solvers and Numerical Methods for Fluid Dynamics: A Practical Introduction, Springer-Verlag, 2009.

[30] B. van Leer, Towards the ultimate conservative difference scheme. V. A second-order sequel to Godunov's method, J. Comput. Phys., 32 (1979), 101-136.

[31] Y. Xing, Exactly well-balanced discontinuous Galerkin methods for the shallow water equations with moving water equilibrium, J. Comput. Phys., 257 (2014), 536-553.

[32] Y. Xing and C.-W. Shu, High order well-balanced finite volume WENO schemes and discontinuous Galerkin methods for a class of hyperbolic systems with source terms, J. Comput. Phys., 214 (2006), 567-598.

[33] Y. Xing, C.-W. Shu, and S. Noelle, On the advantage of well-balanced schemes for moving-water equilibria of the shallow water equations, J. Sci. Comput., 48 (2011), 339-349.

[34] J. G. Zhou, D. M. Causon, C. G. Mingham, and D. M. Ingram, The surface gradient method for the treatment of source terms in the shallow-water equations, J. Comput. Phys., 168 (2001), 1-25.